

Electrical, structural, and chemical properties of HfO₂ films formed by electron beam evaporation

K. Cherkaoui,^{1,a)} S. Monaghan,¹ M. A. Negara,¹ M. Modreanu,¹ P. K. Hurley,¹ D. O'Connell,¹ S. McDonnell,² G. Hughes,² S. Wright,³ R. C. Barklie,³ P. Bailey,⁴ and T. C. Q. Noakes⁴

¹Tyndall National Institute, University College Cork, Lee Maltings, Prospect Row, Cork, Ireland

²School of Physical Sciences, Dublin City University, Glasnevin, Dublin 9, Ireland

³School of Physics, Trinity College Dublin, Dublin 2, Ireland

⁴STFC Daresbury Laboratory, Daresbury, Warrington, Cheshire WA4 4AD, United Kingdom

(Received 7 April 2008; accepted 14 July 2008; published online 24 September 2008)

High dielectric constant hafnium oxide films were formed by electron beam (e-beam) evaporation on HF last terminated silicon (100) wafers. We report on the influence of low energy argon plasma (~ 70 eV) and oxygen flow rate on the electrical, chemical, and structural properties of metal-insulator-silicon structures incorporating these e-beam deposited HfO₂ films. The use of the film-densifying low energy argon plasma during the deposition results in an increase in the equivalent oxide thickness (EOT) values. We employ high resolution transmission electron microscopy (HRTEM), x-ray photoelectron spectroscopy (XPS), and medium energy ion scattering experiments to investigate and understand the mechanisms leading to the EOT increase. We demonstrate very good agreement between the interfacial silicon oxide thicknesses derived independently from XPS and HRTEM measurements. We find that the e-beam evaporation technique enabled us to control the SiO_x interfacial layer thickness down to ~ 6 Å. Very low leakage current density ($< 10^{-4}$ A/cm²) is measured at flatband voltage +1 V into accumulation for an estimated EOT of 10.9 ± 0.1 Å. Based on a combined HRTEM and capacitance-voltage (CV) analysis, employing a quantum-mechanical CV fitting procedure, we determine the dielectric constant (k) of HfO₂ films, and associated interfacial SiO_x layers, formed under various processing conditions. The k values are found to be 21.2 for HfO₂ and 6.3 for the thinnest (~ 6 Å) SiO_x interfacial layer. The cross-wafer variations in the physical and electrical properties of the HfO₂ films are presented. © 2008 American Institute of Physics. [DOI: 10.1063/1.2978209]

I. INTRODUCTION

As the semiconductor industry drives toward smaller device sizes while striving to maintain power consumption at acceptable levels, in particular, for portable applications, the incorporation of new materials becomes inevitable.¹ HfO₂ is a leading candidate among the high dielectric constant (high- k) materials to replace, or be combined with, silicon dioxide in many applications. Amorphous HfO₂ was found to enhance transistor performance in transparent thin-film transistors.² Furthermore, HfO₂ films formed by pulsed laser deposition at low temperature demonstrated suitable properties when incorporated in metal-insulator-metal capacitors for mixed signal integrated circuit applications.³ More significantly, HfO₂ or HfO-based high- k dielectrics with metal gates have recently been introduced into the gate stack of metal-oxide-semiconductor (MOS) field effect transistors at the 45 nm technology node.

Nevertheless, there are still major issues relating to the control of the interfacial silicon oxide that forms at the high- k /silicon interface.⁴ This is of critical importance in ensuring that the equivalent oxide thickness (EOT) of the complete dielectric stack is not dictated by the silicon oxide interfacial thickness. In addition, some fundamental properties

of HfO₂ are still not clearly understood. For example, the origin of electron and hole trapping sites in the bulk of HfO₂ films is still debated,⁵ and the thermal stability of thin-film HfO₂ (< 50 Å) on silicon is another major issue still unresolved.⁶

Growth techniques such as atomic layer deposition (ALD) yield very good quality high- k films.⁶ However, for dielectric materials which evaporate stoichiometrically, the electron beam (e-beam) evaporation technique is a very cost-effective way of investigating the basic chemical and electrical properties of high- k films, as well as providing a route for screening a wide range of potential high- k materials as suitable candidates for gate dielectric applications.⁷ This technique could also help in discriminating between intrinsic properties of the dielectric material and extrinsic material issues such as impurity contamination.

In this study an e-beam evaporation technique has been used to form HfO₂ layers from monoclinic HfO₂ source material. HfO₂ layers with a target thickness in the range of 30–50 Å were deposited on HF last silicon (100) substrates. We combined a wide range of chemical, structural, and electrical characterization techniques to investigate the basic properties of the high- k layers. X-ray photoelectron spectroscopy (XPS) was used to characterize the chemical composition of the HfO₂ film and the HfO₂/Si interfacial chemistry. High resolution transmission electron microscopy (HRTEM)

^{a)}Electroni mail: karim.cherkaoui@tyndall.ie.

was used to independently measure the thickness of the interfacial layer (IL) and the thickness of the HfO₂ overlayer. Electrical characterization in the form of current density-voltage (JV) and capacitance-voltage (CV) measurements was carried out on MOS capacitors fabricated by depositing nickel (Ni) contacts on the HfO₂ layers in order to evaluate the leakage current across the dielectric and in order to calculate the dielectric constant of the HfO₂ film and the interfacial SiO_x layer.

Frequently the e-beam technique involves the use of low energy ions to assist the deposition of the film.⁸ The argon (Ar) ion bombardment of the film during deposition has the potential to densify the high-*k* film during the growth process, reducing the possibility of void formation that would lower the effective *k* value. Optical coatings have significantly benefited from the use of ion assist during film deposition.⁹ In this work, we also investigate the effect of the argon ion-assist process on the physical and electrical properties of the resulting HfO₂/SiO_x/Si(100) structures, with a particular emphasis on the interfacial SiO_x layer thickness between the HfO₂ and the silicon substrate. We will show that the use of an argon ion assist during the film formation results in a thicker IL. A range of experiments are reported, including O₂ with an Ar ion assist, O₂ with no Ar ion assist, and no O₂ with Ar ion assist. The purpose is to determine the process combinations that result in the enhanced IL growth. Experimental results are also presented for the case of a two-stage growth process where direct exposure of the Si surface to the Ar ions is prevented during the e-beam evaporation of a 10 Å HfO₂ film prior to the Ar ion assist being activated for the remaining nominal 15 Å HfO₂ film deposition. The paper demonstrates very good agreement between the interfacial oxide thickness derived independently from XPS, HR-TEM, and electrical measurements. The local surface roughness and the cross-wafer uniformity of the HfO₂ films are assessed by atomic force microscopy (AFM), spectroscopic ellipsometry (SE), and the cross-wafer dispersion of current density versus voltage characteristics.

II. EXPERIMENTAL DETAILS

The HfO₂ layers are formed on *N*- and *P*-type silicon (100) 4 in. wafers (2–4 and 10–20 Ω cm, respectively) by e-beam evaporation. The Si wafers undergo a standard chemical clean and are dipped in HF (10:1 de-ionized water / HF for 10 s) to remove the native Si oxide before being loaded into the e-beam chamber. The wafers are placed on a rotating carousel for improved uniformity. Oxygen can be introduced into the chamber during the deposition at variable flow rates [from 0 up to 7 SCCM (SCCM denotes cubic centimeter per minute at STP)], and low energy (~70 eV) argon ion assist can be employed to densify the HfO₂ films during formation. The Ar⁺ ions are produced by flowing Ar gas across a heated tungsten filament. A bias of 120 V is applied to the anode to accelerate the Ar⁺ ions to the substrate. The base pressure in the chamber is 10⁻⁶ Torr and can rise up to 2 × 10⁻⁴ Torr when both O₂ and Ar are introduced. The source material consists of 3–5 mm monoclinic HfO₂ pellets of 99.99% purity. The Si wafers are heated to 150 °C

during the deposition. The minimum HfO₂ film target thickness was 25 Å, however, the measured physical thickness (as it will be discussed below) was found to be consistently higher (35–40 Å). Control of the precise film thickness of these thin films in an e-beam evaporation system designed to produce much thicker optical films is difficult, however, excellent reproducibility was achieved for the same nominal conditions during repeat depositions. MOS capacitors with a range of gate areas were subsequently fabricated using photolithography and a lift-off process. Results are presented for 55 × 55 μm² MOS structures. The metal gate consists of 300 nm of Ni deposited *ex situ* by e-beam. Nickel was selected as a high work function gate metal since the experimental matrix did not include high temperature (>450 °C) post-metal-thermal budgets. The XPS analysis of the samples was carried out in a VG Microtech electron spectrometer at base pressures of 2 × 10⁻⁹ and 1 × 10⁻¹⁰ Torr in the preparation and analysis chambers, respectively. The photoelectrons were excited with an Al Kα x-ray source (*hν* = 1486.6 eV), and the pass energy of the analyzer was 20 eV, yielding a resolution of 1.2 eV. The Hf 4*f*, O 1*s*, Si 2*p*, and C 1*s* peaks were recorded along with 20–1000 eV survey scans at 0° and 35° with respect to the surface normal. The intensities of the peaks were determined as the integrated peak areas assuming an integral “Shirley” background. All the samples are thin enough to detect the XPS signal from the full stack down to the silicon substrate, and no thinning by dilute HF etching was necessary. We have also applied the medium energy ion scattering (MEIS) technique to gain more information on the depth dependence of the film stack chemistry. The MEIS data consist of two dimensional maps of scattered ion intensity where the two coordinates are the scattered ion energy and the scattering angle for a given incidence of the 100 keV He⁺ ion beam. More experimental details of this technique are described in depth in Ref. 10. The scattering geometry used is an incidence angle of 54.7° (corresponding to ⟨111⟩ in) and a scattering angle of 90° (corresponding to ⟨211⟩ out). This geometry was chosen to minimize the substrate contribution and emphasize the amorphous overlayers. In this study we only analyze the energy spectra, and we largely ignore the crystallographic information since it is not relevant in the case of the amorphous film stacks investigated in this work. SE measurements were carried out using a phase modulated spectroscopic ellipsometer in the spectral range between 1.5 and 6.5 eV at an angle of incidence of 70.30°. The HfO₂ samples are modeled with a five phase system (from top to bottom): the incident medium (air), the surface roughness layer, the HfO₂ layer, the silicon oxide interlayer, and the Si substrate. The thickness of the interlayer between the HfO₂ film and the Si substrate was fixed to the value obtained from HRTEM measurements. The measurements have been performed on eight different points on the wafer. At each point the probed area (beam size) was approximately 1 × 3 mm².

III. RESULTS AND DISCUSSION

Table I summarizes the deposition conditions for the set of samples used in this study (influence of ion assist: A, B, C,

TABLE I. List of samples and process parameters used in this study.

Sample ID	Deposition conditions		
	O ₂ flow (SCCM)	Ar ion assist	Nominal thickness
Impact of ion assist			
A	7	No	25 Å
B	7	2 stage	10 Å no ion assist +15 Å ion assist
C	7	Yes	25 Å
D	0	No	25 Å
Impact of oxygen flow			
1	0	Yes	25 Å
2	2.5	Yes	25 Å
3	5	Yes	25 Å

and D; influence of oxygen flow: 1, 2, and 3). Figure 1 shows typical high frequency *CV* characteristics measured on a $55 \times 55 \mu\text{m}^2$ area *N*-type MOS capacitor (two measurement frequencies: 100 Hz and 1 MHz) from sample A. The figure also includes two *CV* characteristics (same measurement conditions) measured on sample A after forming gas annealing (FGA) at 400 °C for 30 min (N_2/H_2 95%/5%) and a simulated quantum-mechanical (QM) *CV*.^{11,12} The theoretical curve that presents the best fit to the measured capacitance between weak inversion and strong accumulation after FGA was obtained for an EOT of $10.9 \pm 0.1 \text{ \AA}$. The measured experimental *CV*s (as-deposited sample) presented in Fig. 1 are not ideal characteristics. However, they are presented to illustrate several issues regarding the formation of high-*k* dielectric layers at low temperature (150 °C). The *CV* stretch-out observed in the as-deposited sample, as compared to the annealed sample, could be attributed to charge build up in the oxide as the *CV* sweep is carried out. This charge could screen the applied field across the oxide and result in lower carrier concentration at the silicon surface than theoretically expected at a given gate voltage. The effect of this charge build up on the leakage currents across the MOS capacitors will be discussed. In addition to the reduced slope,

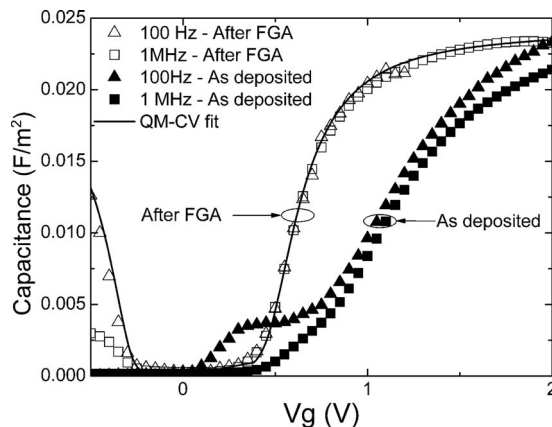


FIG. 1. 100 Hz and 1 MHz capacitance-voltage characteristics measured on sample A as-deposited and after FGA at 400 °C for 30min in N_2/H_2 95%/5%. The line in bold is the QM *CV* fit. Although the *CV* slopes in depletion and into accumulation differ for pre-FGA and post-FGA samples, the flatband voltage remains at $V_{\text{gate}} \sim 0.3 \text{ V}$.

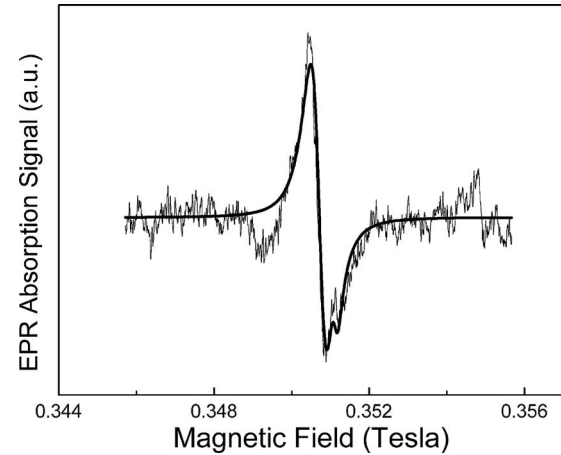


FIG. 2. EPR spectrum at room temperature for a nominal 3 nm HfO_2 on Si(100) in the as-grown state. The deposition conditions are as for sample A. The magnetic field is parallel to the [100] surface normal. The smooth curve shows the fit. The dominant signal at $g=2.0060$ is from P_{b0} ; the signal from P_{b1} at $g=2.0036$ is barely visible.

the *CV*s exhibit significant frequency-dependent dispersion in the depletion region ($V_g \sim 0.5 \text{ V}$), an effect that is attributed to defect states at the oxide/Si interface located at a specific energy in the band gap.¹³ Apart from the annealed sample A, all the results presented in this study were obtained from samples that experienced very low thermal budgets (maximum temperature=150 °C). Evidence has been provided in previous work that Si dangling bonds (P_b centers) are the dominant defect at the oxide/Si(100) interface responsible for the frequency-dependent dispersion of the *CV* in depletion for HfO_2 -based MOS structures with no thermal budget following the HfO_2 deposition.¹⁴ It was also demonstrated that these interface states can be passivated by annealing in forming gas (95% N_2 /5% H_2) at 400 °C.¹⁵ P_b centers induce two discrete energy levels within the Si band gap (within both upper and lower gaps), the energy state P_b (0/-) contributing to the *CV* frequency dispersion observed on the *N*-type wafers (Fig. 1) is located at 0.29 eV above midgap.^{16,17} The *N*-type wafers (2–4 Ω cm) employed in this study have a Fermi level also located at $\sim 0.3 \text{ eV}$ above the intrinsic level. This implies that the interface state electrical response (capacitance or conductance) is highest at, or very close to, the flatband voltage (V_{fb}).

Previous *CV* measurements on a sample prepared under conditions identical to those used for sample A gave an interface state peak density of $2.7 \times 10^{12} \text{ cm}^{-2} \text{ eV}^{-1}$ and an integrated density of $0.73 \times 10^{12} \text{ cm}^{-2}$ extracted from a 10 kHz *CV*.¹⁴ Electron Paramagnetic Resonance (EPR) measurements on another identically prepared sample shown in Fig. 2 give a total P_{b0} plus P_{b1} concentration of $(1.5 \pm 0.5) \times 10^{12} \text{ cm}^{-2}$ with approximately 95% of this due to the P_{b0} centers. EPR spectra were recorded at room temperature with the field applied along the [100] surface normal and parallel to [011] in the film plane. Figure 2 also shows the fit for the field along the surface normal. The spectrum is dominated by the P_{b0} line at $g=2.0060$, with that due to P_{b1} at $g=2.0036$ barely visible. The large P_{b0}/P_{b1} ratio is typical of the (100)Si/SiO₂ interface grown at low temperatures.¹⁸ A good match between the densities of interface states and P_b centers

TABLE II. Summary of EOT and k values for the HfO_2 films and the ILs extracted from the QM CV fits of the CV data. The reported k values represent the median values of the range of possible k values for each process.

Sample	EOT	$k(\text{SiO}_x)$ interlayer	$k(\text{HfO}_2)$ oxide
A	10.9 ± 0.1 Å	6.3 ± 1.7	21.5 ± 3.5
B	25.6 ± 0.3 Å	4.2 ± 0.3	19.0 ± 3.0
C	33.1 ± 0.5 Å	4.3 ± 0.2	23.0 ± 2.0

has been recorded before for HfO_2 films grown on Si(100) by metal organic chemical vapor deposition.¹⁹

It is interesting to note that in Fig. 1 the FGA not only reduces the interface state density but also removes the stretch out. This is evident from Fig. 1 since the simulated CV matches very well the experimental data after FGA across the full bias range. It is yet to be clarified whether this charge trapping effect is removed by hydrogen passivation of oxide bulk defects or whether it is eliminated by the temperature annealing regardless of the ambient. It is, however, clear that the FGA did not cause any EOT increase, i.e., there is no IL regrowth under these annealing conditions, since the maximum capacitance is not changed after FGA.

Samples where the HfO_2 films were formed with the Ar ion assist (either throughout the deposition or in a two-stage deposition process in the case of sample B) presented considerably higher EOT values. Table II summarizes the EOT values for samples A–C. These values were extracted similarly to sample A from the QM CV characteristics corresponding to the maximum capacitance in strong accumulation (not shown). Based on the amplitude of the CV frequency dispersion observed on samples B and C, the interface state density is also larger for samples B and C than for sample A. Ions impinging on the Si(100) bare surface will create defects inducing measurable effects by CV even at energies as low as 70 eV. It was demonstrated previously that 60 eV argon ions can create a thin amorphous layer on Si(100) samples.²⁰ It is interesting to note that the 10 Å HfO_2 layer deposited prior to initiating the ion assisted growth does not prevent the damage at the Si/SiO_x interface (sample B). In order to understand the EOT values, HRTEM was performed on three samples (A–C). The high resolution cross-sectional images (Fig. 3) show clear bilayer stacks on all three samples. The HfO_2 films have physical thicknesses in the range of 37–40 Å. The achieved physical thicknesses are within the useful thickness range for high- k gate oxide studies. In addition, the deposited HfO_2 films seem to be amorphous under our deposition conditions. Figure 3 also shows an increasing IL physical thickness from 6 Å in sample A to 29 Å in sample C. It should be noted that an enhanced IL thickness of 19 Å is still present when the Si surface is protected by a 10 Å thick HfO_2 layer before turning on the Ar⁺ ion assisted deposition (sample B). Table II also includes k values extracted from the QM CV measurement fits to experimental measurements. The method of extraction first assumes that the HRTEM images give accurate thickness estimates for all three samples [sample A: $t(\text{SiO}_x) = 6$ Å, $t(\text{HfO}_2) = 37$ Å; sample B: $t(\text{SiO}_x) = 19$ Å, $t(\text{HfO}_2) = 37$ Å; sample C: $t(\text{SiO}_x) = 29$ Å, $t(\text{HfO}_2) = 40$ Å]. The sec-

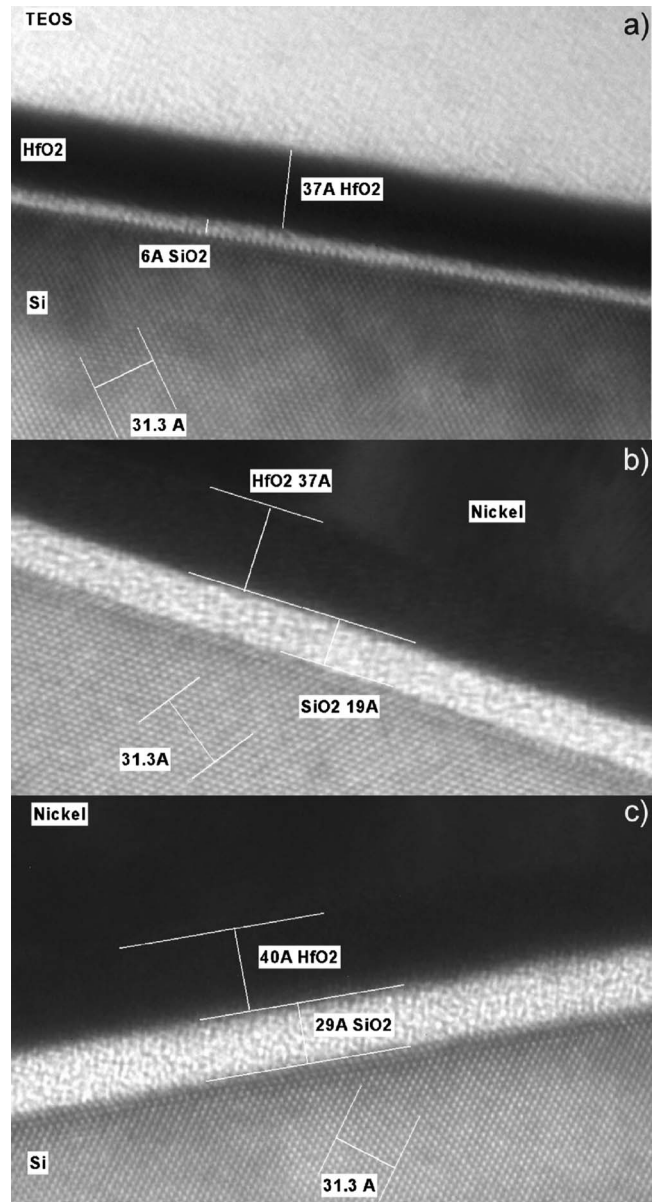


FIG. 3. HRTEM cross sections showing the increase in the IL layer from (a) no ion assist deposition +O₂ (sample A), (b) two-stage deposition +O₂ (sample B), and (c) ion assist throughout the deposition +O₂ (sample C).

ond assumption is that the k value for the hafnium oxide layer falls within the range of 16–25. The third assumption is that the k value for the IL is in the range of 3.9–8.0. We regard these three assumptions as very reasonable. All combinations of possible k values were sampled during the EOT extraction, narrowing the range of possible k values and EOTs. The EOT extractions for samples B and C were taken from the maximum capacitance measurements in strong accumulation. Sweeping the possible k values for both layers in each sample yields EOT values of 25.6 ± 0.3 Å for sample B and 33.1 ± 0.5 Å for sample C. The possible range of k values was extracted as $k(\text{SiO}_x) = 4.2 \pm 0.3$ and $k(\text{HfO}_2) = 19 \pm 3$ for sample B and $k(\text{SiO}_x) = 4.3 \pm 0.2$ and $k(\text{HfO}_2) = 23 \pm 2$ for sample C. In sample A, the EOT is extracted from the QM CV fit from weak inversion to strong accumulation. The three assumptions yield an EOT of 10.9 ± 0.1 Å

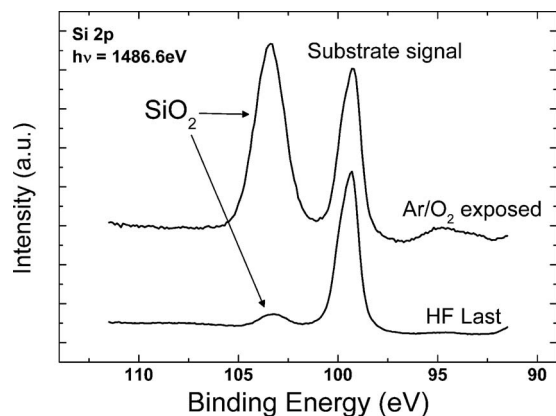


FIG. 4. XPS spectrum of a silicon wafer exposed to Ar ions during the stabilization time prior to the HfO₂ layer deposition compared to the spectrum of a blank Si wafer after HF dip and not subjected to the Ar ions (the HfO₂ film deposition was not carried out on these samples).

for a range of k values $k(\text{SiO}_x)=6.3 \pm 1.7$ and $k(\text{HfO}_2)=21.5 \pm 3.5$. The mean k for HfO₂, obtained from the three median values (21.5, 19.0 and 23.0) is 21.2.

The higher k (6.3 ± 1.7) value for the IL of sample A compared to the other samples, which are closer on average to the SiO₂ value (3.9), could be explained by the formation of a substoichiometric interfacial oxide in sample A. The deposition temperature (150 °C) is too low to favor the growth of stoichiometric SiO₂. Although there is only limited knowledge regarding the electrical properties of subnanometer SiO_x layers, it was previously demonstrated that even for thermally grown SiO₂ layers, the initial 6 Å of the silicon oxide layer at the Si interface is predominantly substoichiometric.²¹ This is supported by theoretical predictions showing a k value of 6–7 for a 6 Å interfacial substoichiometric SiO_x layer between Si(100) and 17 Å of SiO₂. Our extracted median k value for sample A is 6.3, within the range of 6–7 predicted by theory.²² In general, the k values for all samples span a significant range, albeit reduced from the initially assumed ranges in most cases. Nevertheless, the range of extracted EOT becomes smaller as we move from sample C (± 0.5 Å) to sample A (± 0.1 Å).

It could be hypothesized that the thick IL is formed during the exposure of the Si surface to O₂ and Ar⁺ ions during the e-beam stabilization time prior to HfO₂ deposition. In order to unambiguously establish how this IL forms, a HF last silicon wafer was exposed to the argon ions and the oxygen gas for 3 min in the chamber prior to e-beam evaporation without proceeding with the HfO₂ deposition step. This is the normal time necessary to stabilize the e-beam system before starting the HfO₂ deposition, when the silicon wafer is exposed to the Ar ion assist and the oxygen ambient. Figure 4 shows the XPS Si 2p spectrum recorded on this wafer. The difference between the silicon surface which was subjected to the procedure compared to the control wafer which was measured following HF last treatment and exposed to atmospheric conditions for the same length of time prior to measurement is evident. These spectra clearly show that the bulk of the IL, which has a thickness of the order of 30 Å, grows in the initial stabilization phase prior to dielectric deposition. From combined CV and XPS analysis it was

established that the IL thickness is reduced by ~ 10 Å when the O₂ flow rate is decreased from 7 to 2.5 SCCM in the presence of Ar⁺ ion assist. In addition, previous XPS measurements recorded on HfO₂ films formed by e-beam using Ar⁺ ion assist under varying O₂ flow rates demonstrated a very thin (< 6 Å) IL when O₂ was absent.²³ It is therefore the combined presence of oxygen and low energy Ar⁺ ions during the deposition procedure that results in such significant SiO₂ layer formation. One can speculate about the mechanisms by which the IL formation is enhanced. The low energy Ar⁺ ions modify the Si surface and probably make it more reactive. In addition, the Ar plasma process will cause the formation of O radicals, resulting in the formation of an oxide layer through a process of low temperature plasma oxidation.^{24,25} The presence of ~ 20 Å of interfacial SiO₂ in the case of sample B also demonstrates that O₂ molecules or oxygen radicals can diffuse through 10 Å of HfO₂ at low temperature (150 °C). Relatively thick SiO₂ IL formation during HfO₂ deposition using reactive sputtering in Ar/O₂ ambient has already been observed previously.^{26–28} In all studies, the IL thicknesses, 25, 28, and 32 Å, respectively, are very close to the IL thickness (30 Å) of the current work for HfO₂ films formed in O₂ ambient and with the ion assist on (samples C, 2, and 3). This indicates that in the presence of Ar/O₂ plasma and in low temperature conditions [from 24 °C (Ref. 26) to 100 °C (Ref. 28)] the oxidation process results in a typical IL thickness around 30 Å. The IL thickness is further increased (from 25 to 36 Å) when the substrate temperature is raised to 500 °C.²⁶ Yamamoto *et al.*,²⁷ however, managed to reduce the IL thickness by forming a Hf metal layer preventing oxidizing species from diffusing to the Si interface during the deposition. This Hf metal layer must be engineered to be entirely oxidized otherwise the presence of metallic Hf deteriorates the electrical properties.

In a different study Choi *et al.*²⁹ used a similar approach to demonstrate the catalytic nature of Hf metal on Si. The authors showed using the e-beam evaporation technique that depositing a thin HfO₂ layer from HfO₂ pellets in O₂ ambient resulted in an IL less SiO₂-like than when the HfO₂ film was formed from Hf metal in the same O₂ ambient. They concluded that the presence of Hf–Si bonds during the deposition resulted in more Si–O bonds. Hence, the Si surface should not be exposed to Hf and oxygen at the same time to limit the IL formation during deposition by e-beam.

Sample A (no ion assist and O₂ ambient) and sample 1 (ion assist and no O₂ flow), which both have comparable IL thicknesses of ~ 6 Å, provide further evidence that a combination of an O₂ ambient and an Ar ion assist during deposition is required to result in the formation of a thick IL. However, while the XPS data obtained on both samples present comparable IL thicknesses (Fig. 5), the electrical properties of the two films are entirely different. Figure 6 shows the leakage current density of MOS capacitors fabricated on the two wafers. The JV characteristics point to a short between the gate electrode and the substrate for the sample using the ion-assist process without O₂. To understand the origin of these poor electrical properties, a third experiment (sample D) was performed where both the O₂ and the ion assist were suppressed. The JV characteristics of

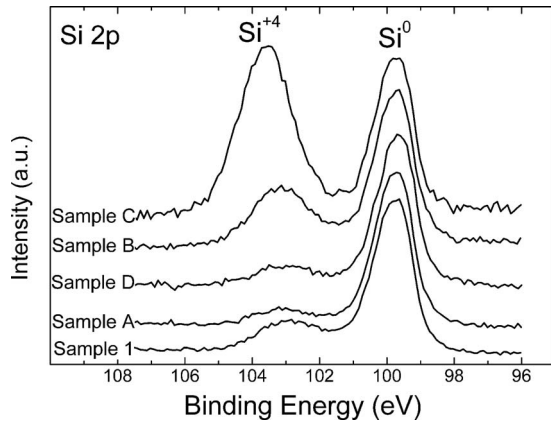


FIG. 5. Si 2*p* XPS spectra for several samples investigated in this study. The Si⁴⁺ signal indicates the IL thickness variation under different deposition conditions. Note the increase in the IL thickness when both O₂ and the Ar ion assist are present during the deposition (samples B and C).

sample D are compared to samples A and 1 in Fig. 6, and it is very similar to sample A (but with slightly better insulating properties resulting from the increased EOT value of 15 Å). The IL layer of sample D evaluated by XPS was found to be similar to samples A and 1 (Fig. 5). This last experiment demonstrates that the O₂ ambient is not a necessary condition to obtain good insulating properties for HfO₂ films formed by e-beam and confirms that the use of ion assist without oxygen is responsible for the poor electrical characteristics (sample 1).

Figure 7 shows the core level XPS spectra for the Hf 4*f* and the O 1*s* for different samples (A–C). We have also included the XPS spectra measured on HfO₂ layers deposited on HF last silicon (100) wafers under varying oxygen flow rates (samples 1–3). The asymmetry in the O 1*s* peak is due to the presence of a chemically shifted oxygen component at higher binding energy which has been attributed to surface absorbed oxygen. The spectra show that the energy separation between the Hf 4*f* 7/2 and the O 1*s* peaks is independent of oxygen flow rate and remains constant at 513.7 ± 0.1 eV, which is the separation found for a pure HfO₂ powder sample measured by the same spectrometer. This is direct evidence that the changing oxygen flow rate did not affect

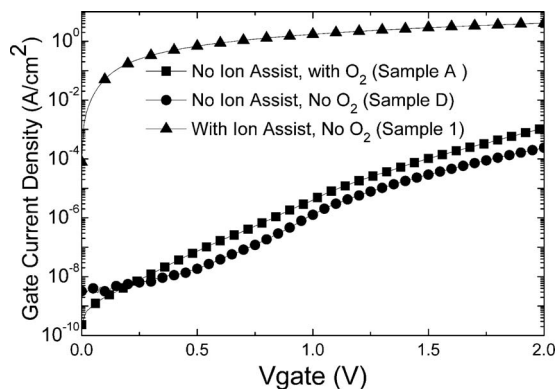


FIG. 6. Oxide leakage current density vs gate voltage for sample A, showing very similar leakage characteristics to HfO₂ films deposited under no O₂ and no ion assist (sample D). The leakage current of a HfO₂ film deposited under no O₂ and ion assist (sample 1) is also shown. All three films have the same HfO₂ target thickness of 25 Å.

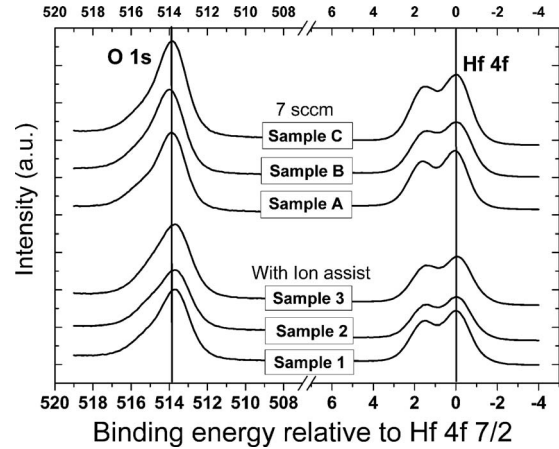


FIG. 7. Hf 4*f* XPS spectra for samples A–C compared to samples deposited under variable O₂ flow (samples 1–3).

the chemical state of the elements in the HfO₂ film, since the presence of metallic hafnium or hafnium silicide would alter this energy separation by introducing different chemically shifted peaks. The presence of substoichiometric HfO_(*x*<2) would give rise to additional peaks in the Hf 4*f* spectrum as reported by Cho *et al.*³⁰ for pulsed laser deposition of HfO₂ in an oxygen deficient environment. Using the conventional relative sensitivity factors (RSFs) for the two elements and the peak areas,³¹ the hafnium to oxygen concentrations for all samples were determined to be in the ratio of 1:2 (Hf:O) to within 3%. This confirms that, within experimental error, the film composition is constant and independent of oxygen flow within the investigated range. In addition, the peak profile and energy position of the Hf 4*f* and the O 1*s* peaks for the three different procedures (A–C) shown in Fig. 7 indicate that the HfO₂ deposits stoichiometrically independent of the processing sequence used. Hence, the stoichiometry of the HfO₂ film in sample 1 is not the cause of the poor insulating properties observed in Fig. 6.

The next part of the study involves measuring the thickness of the IL that forms at the interface when the HfO₂ layer is deposited. By comparing the relative areas under the SiO₂ IL signal (seen at ~103 eV binding energy) and the Si bulk signal, it is possible for changes in the interfacial oxide thickness to be monitored. Vitchev *et al.*³² have used this approach to evaluate the interfacial silicon oxide thickness on silicon for HfO₂ and Al₂O₃ overlayers. Seah and Spencer³³ used an extended approach for SiO₂ on Si to examine the influence of substoichiometric silicon oxide on the dielectric thickness determinations. Equation (1) is the basic equation used for an analysis of a SiO₂ IL,

$$\ln \left[1 + \frac{R_{\text{exp}}}{R_0} \right] = (L_{\text{SiO}_2})^{-1} d \sec \theta. \quad (1)$$

Equation (1) relates the SiO₂ thickness (*d*) to the SiO₂ signal, where *R*_{exp} is the ratio of the area under the Si⁴⁺ peak to that of the Si⁰ and *R*₀ is the same ratio for an infinitely thick pure SiO₂ sample and a pure silicon sample. The value of *R*₀ was taken from Ref. 34 to be 0.82 and is thus single valued in this analysis, excluding the contributions from substoichiometric silicon oxide. *L*_{SiO₂} is the electron attenuation length of an

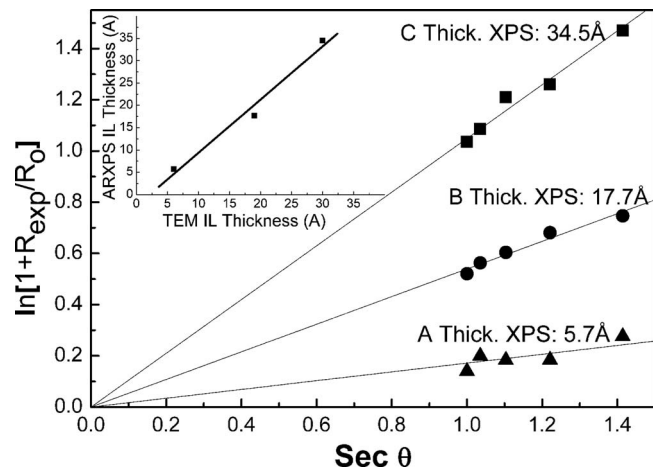


FIG. 8. ARXPS analysis and the corresponding extracted IL thickness. The inset shows the IL thickness extracted from ARXPS vs IL thickness obtained from HRTEM.

electron originating from a silicon atom in SiO_2 and the average value of 33 \AA was taken for L_{SiO_2} . Since both the substrate and the SiO_2 layer are attenuated equally by an overlayer,³² Eq. (1) can be used to accurately estimate the interfacial oxide layer thickness in a high- $k/\text{SiO}_2/\text{Si}$ system. When the IL has substoichiometric contributions, the Eq. (1) estimate will be less accurate and therefore should be considered in conjunction with the HRTEM estimates. Figure 8 shows the results of an angular XPS study carried out to determine the thickness of the interfacial silicon oxide layer from the slope of $\ln(1+R_{\text{exp}}/R_0)$ versus $\text{sec } \theta$ for three different samples (A–C). This results in the determination of the interfacial oxide as 5.7 \AA in the case of sample A, 17.7 \AA thick with the two-stage deposition (sample B), and 34.5 \AA with the ion assist (sample C). The quantitative agreement between the thickness values of the interface oxide layer as determined using XPS and HRTEM measurements, shown as an inset in Fig. 8, supports the use of pure SiO_2 values for L_{SiO_2} and R_0 in Eq. (1) of the XPS analysis.

To gain more understanding of the composition of the $\text{HfO}_2/\text{SiO}_x/\text{Si}$ structures, and to elucidate factors that could influence the leakage current density, the samples were analyzed by the complementary technique of MEIS. Figure 9 shows the MEIS spectra measured on samples A–C and 1. Each spectrum corresponds to a cross section taken at a constant scattering angle of 90° in the two dimensional data. The spectra show very similar peaks for the main elements (Hf, Si, and O) present in the three different films. All samples present a high background signal spanning from low energy to the high energy side of the Si peak. It is interesting to note that the background signal increases from sample A to sample C probably as a consequence of the IL thickness increase. It is believed that the high dechanneling seen for 100 keV He^+ ions passing through a high Z number overlayer such as Hf is due to multiple scattering within the layer. The broadening of the O peak for sample C seems to support this argument. The peak around 80 keV is attributed to argon, which is clearly present in the spectra of samples B and C (Ar ion assist either used partially or fully). The double feature of the Ar peak in sample C suggests that it is located in

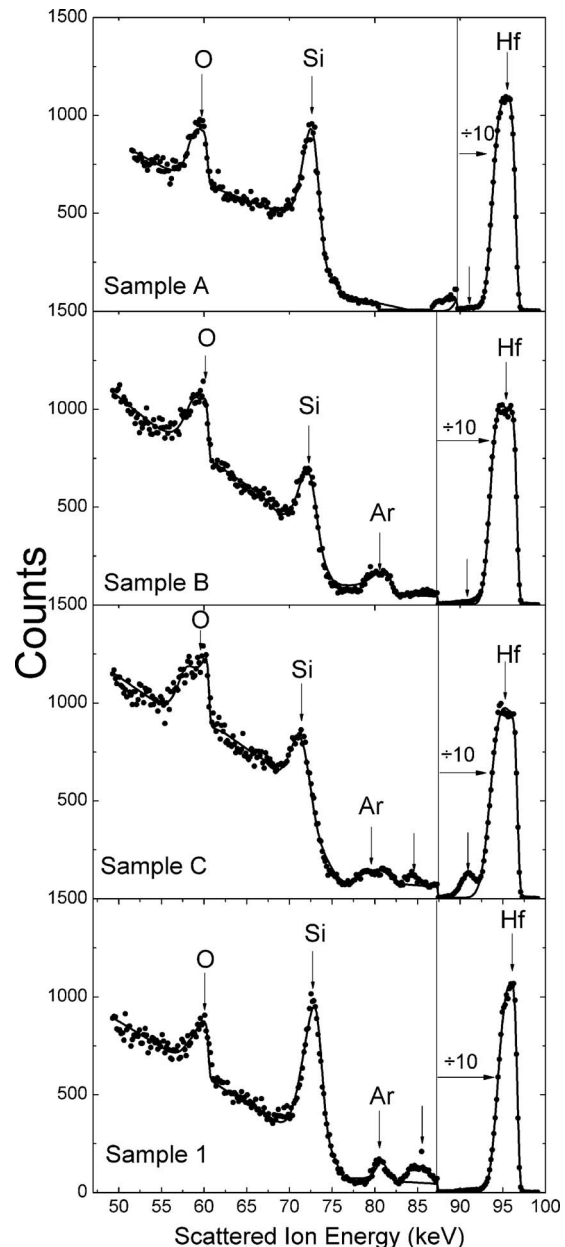


FIG. 9. Scattered ion energy spectra obtained from MEIS experiments on samples A–C and 1. The incidence angle is 54.7° ($\langle 111 \rangle$) and the scattering angle is 90° ($\langle 211 \rangle$). The unlabeled arrows indicate peaks due to impurity contamination. The dotted curves are the experimental data and the solid lines are the simulated spectra assuming the parameters of Table III.

two distinct layers (possibly SiO_2 and HfO_2). Another peak occurring at around 85 keV is difficult to ascribe. It could be a contaminating impurity, yet it is only present when the ion assist is used during the deposition and the peak intensity is very much reduced in sample B. Another very interesting feature is the low energy tail of the Hf peak. It could be attributed to zirconium (Zr), an element always present in HfO_2 source material. However, the same source material was used for all depositions, and the presence of a sharp peak at the same energy in the spectrum of sample C seems to contradict this explanation. Another possible explanation could be the presence of Hf in the SiO_2 IL. Such Hf diffusion could be enhanced by the ion assist, which could explain why we see it reduced in samples A and B, with the presence

TABLE III. HfO₂ and IL thickness values extracted from the fit of the MEIS spectra experimental data. The IL thickness values include a displaced Si⁰ layer at the Si interface with the oxide.

Sample	HfO ₂ width (Å)	IL width (including displaced Si ⁰) (Å)	Ar (at. %)	Peak at 85 keV
A	35	29	0	None
B	42	32	0.03	Small
C	41	41	0.019	Larger
1	36	58	0.04	Largest

of a tail rather than a peak in the spectra. However, this explanation is, in fact, unlikely, since it was not possible to fit the MEIS spectrum when it is assumed that Hf is present in the IL.

Depth profiles were extracted from MEIS experiments to fit the energy spectra using a model with an energy-dependent and composition-dependent stopping power, an Andersen screening correction, and an empirical straggling value. Stopping powers were calculated from SRIM 2005 using a bulk density for HfO₂ and an SiO₂ density 88% of bulk. The model is based on a three or four layer system. The simplest three layer model has layer one containing Hf/Si/O, layer two Si/O, and layer three just Si (the latter layer accounts for Si⁰ displacement at the SiO₂/Si interface). A four layer model is needed for the samples containing Ar. When comparing the layer thicknesses as determined by MEIS and HRTEM it should be noted that, in an aligned geometry, the signal MEIS “sees” atoms that are moved from the bulk lattice site by more than ~10% of the interatomic distance (along the ⟨111⟩ direction), i.e., >0.023 nm, while the HRTEM thicknesses are evaluated from atomic number contrast. Hence, the IL thickness in Table III is the thickness sum of the silicon in the SiO_x layer and the displaced Si⁰ layer at the SiO_x/Si interface. HRTEM does not distinguish between displaced Si⁰ and nondisplaced Si⁰, therefore no thickness contribution from this region is visible by HRTEM. The results of the MEIS modeling are summarized in Table III. The differences between MEIS and HRTEM data are evident for the extracted IL thickness, in particular, for samples A and 1, indicating that the displacement of the silicon substrate atoms is more significant in these two samples.

The MEIS results in Table III could explain the poor electrical properties of sample 1 (see Fig. 6), which has the thickest IL deduced from MEIS. A possible mechanism for the enhanced leakage measured in this sample is the damaged Si surface by Ar⁺ ions, which is not oxidized in the absence of O₂ during the deposition.

Unlike ALD, the e-beam technique is a nonconformal deposition method unsuitable for high aspect ratio step coverage. However, the films obtained by this technique display outstanding uniformity on planar 100 mm diameter silicon wafers. This outstanding uniformity reinforces the argument for the e-beam technique as a method of choice for screening high-*k* dielectrics and investigating fundamental material properties. The uniformity of the films is illustrated in the gate leakage current density versus voltage (*JV*) plots of Fig. 10 (sample A, area=55 × 55 μm², *T*=25 °C). The measured

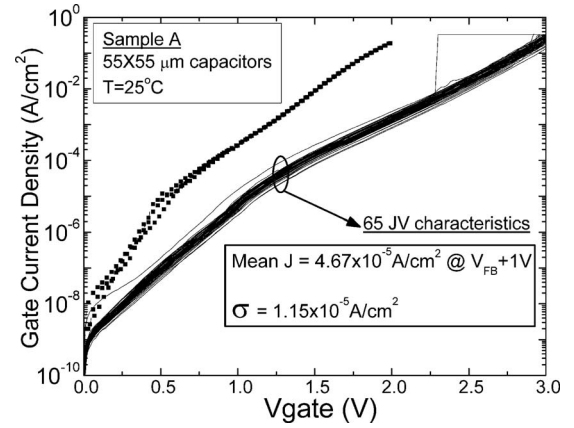


FIG. 10. 65 *JV* characteristics measured on 55 × 55 μm² MOS capacitors of sample A at 25 °C. The dotted curves are the measured *JV* characteristics after FGA.

JVs (65 in total), taken at any given voltage, always spread over less than one order of magnitude. In the direct tunneling regime, this translates into a thickness variation of less than 2 Å.³⁵ The CVs of Fig. 1 indicate that the flatband voltage (*V*_{fb}) is at *V*_{gate} ~ 0.3 V. Hence, *V*_{fb} + 1 V into accumulation for the plotted *JVs* is at *V*_{gate} ~ 1.3 V. Over 90% of the *JV* characteristics give a leakage current density below 6 × 10⁻⁵ A/cm² at *V*_{fb} + 1 V, confirming the excellent insulating properties of these thin films. The *JVs* of Fig. 10 present two distinct regions. At low voltage (<1 V), the current transport through the film stack is dominated by defect-enhanced mechanisms and was found to be highly temperature dependent. The higher voltage region (>1 V) is dominated by the mechanism of direct tunneling. It is pointed out that theoretical simulations are able to match the rate of the current increase with voltage for |*V*| > 1 V. However, the absolute amplitude of the measured current for sample A prior to FGA at 400 °C (Fig. 10) is approximately two orders of magnitude lower than the simulated *JVs* based on direct tunneling¹. While thinner EOT HfO₂ films have been demonstrated using e-beam technique,⁷ such a low leakage current is unusual. This behavior could be explained similarly to the evolution of the CV characteristics of Fig. 1 before and after FGA. As discussed earlier in terms of the CV response (Fig. 1), the samples prior to the FGA process exhibit bulk charge trapping and a significant interface state density (~1 × 10¹² cm⁻²). The bulk and interface charge will reduce the density of electrons in the accumulation region for a given applied gate voltage, resulting in the abnormally low leakage for the as-deposited (low thermal budget) film. This explanation is supported by the results in Fig. 10, which indicate that the leakage current density does increase following the FGA at 400 °C to values around 2 × 10⁻³ A/cm² at *V*_{fb} + 1 V into accumulation, in agreement with the theoretically predicted current density by direct tunneling.¹

¹The simulated *JV* is based on an ~6 Å SiO_x and an ~37 Å HfO₂ composite layer with tunneling effective masses of 0.5*m*₀ and 0.11*m*₀ in the SiO_x and HfO₂, respectively, and electron affinities of 1.75 and 1.4 eV for the HfO₂ film and SiO_x layer, respectively. The Ni gate work function is ~4.71 eV. This yields a value of ~1 × 10⁻³ A/cm² at *V*_{fb} + 1 V.

TABLE IV. HfO₂ surface roughness and film thickness measured by AFM and SE. The thickness obtained by SE is higher than that obtained by HRTEM. The cross-wafer film uniformity is better than 1 Å. The AFM rms value is an average of six measurements from six separate 1 × 1 μm² areas.

	AFM rms (Å)	HfO ₂ thickness by SE (Å)
A	0.95	46.9 ± 0.2
B	...	53.4 ± 0.6
C	0.98	41.7 ± 0.5

The film surface roughness over 1 × 1 μm² area was measured using AFM. Typical rms values are in the range of 0.95–0.98 Å, and Table IV summarizes the results obtained. The rms values are significantly lower than previously reports by reactive sputtering.²⁸ Uniformity of the HfO₂ film thickness across the wafer was also examined by SE, and the results obtained are also presented in Table IV. The extracted thicknesses for HfO₂ layers are thicker than those obtained by HRTEM (Fig. 3). However, cross-wafer uniformity is excellent and shows a standard deviation of less than 1 Å, demonstrating the ability of our e-beam evaporation technique to grow atomically smooth and uniform thin films.

IV. CONCLUSION

In this work we present a detailed study of the structural, chemical, and electrical properties of high dielectric constant HfO₂ films formed on a HF last terminated silicon (100) surface using an e-beam evaporation technique from monoclinic HfO₂ pellets at 150 °C. In particular, we report the influence of argon ion assist and oxygen flow on the properties of the resulting HfO₂/SiO_x/Si structures, and we explore the thickness variations in the interfacial SiO_x layer with and without argon ion assist and oxygen flow. As observed in other work based on reactive sputtering, the samples involving an argon ion assist (~70 eV), with additional oxygen, result in ~30 Å of interfacial SiO_x. We demonstrate that by using a two-stage process based on an initial growth (~10 Å) with no ion assist, and a subsequent argon ion assisted growth (~15 Å), the interfacial SiO_x layer reduces to ~20 Å. For e-beam evaporation with oxygen flow and without argon ion assist, we obtain an interfacial SiO_x layer of ~6 Å, as determined by HRTEM analysis. Using a systematic QM CV fitting approach, we determine the median dielectric constants to be 6.3, 4.2, and 4.3 for the ~6, ~20, and ~30 Å IL thicknesses, respectively. Although the possible *k* value ranges can be large, the error margins for the EOT extractions are low, from ±0.1 Å for sample A to ±0.5 Å for sample C. Based on XPS analysis, we can confirm that the interfacial silicon oxide layer growth occurs during a stabilization period of argon ion-assisted growth in the presence of oxygen, prior to HfO₂ deposition. In addition, we establish from XPS of the e-beam deposited HfO₂ films that the energy separation between the Hf 4*f* 7/2 and the O 1*s* peaks is independent of the oxygen flow rate, or of the ion-assist process, and remains constant at 513.7 ± 0.1 eV. This is the separation found for a pure HfO₂ powder sample measured by the same spectrometer, confirm-

ing that the HfO₂ films are stoichiometric. Using angle-resolved XPS, it is demonstrated that the interfacial SiO_x thickness is in agreement with the HRTEM analysis to within experimental measurement error. This analysis is complemented by MEIS experiments providing accurate information regarding the chemistry of the IL and depth profile of the film stacks, as well as demonstrating the presence of Ar in the films formed with the argon ion assist. Electrical measurements based on Ni/HfO₂/SiO_x/Si(100) structures yield very low leakage current densities (<10⁻⁴ A/cm²) measured at 1 V above the flatband voltage into accumulation for an EOT of ~10.9 Å. The thickness uniformity of the HfO₂ films over varying length scales is determined by AFM, SE, and current density versus voltage analysis. Surface roughness values from AFM are measured as 0.95 and 0.98 Å for samples A (no ion assist) and C (ion assist), respectively. These results demonstrate the potential of the e-beam deposition technique to form suitable low EOT films for investigating fundamental properties of thin HfO₂ layers and to screen other alternative high-*k* dielectric candidates for MOS applications.

ACKNOWLEDGMENTS

The authors would like to thank Robert Dunne, Stephen Cosgrove, and Jason Roche from Intel Ireland for the TEM and AFM analysis. The authors would also like to thank Science Foundation Ireland (Grant No. 05/IN/1751) and the Engineering and Physical Sciences Research Council, U.K. for the financial support of this work.

- ¹H. Wong and H. Iwai, *Microelectron. Eng.* **83**, 1867 (2006).
- ²K. Nomura, H. Ohta, K. Ueda, T. Kamiya, M. Hirano, and H. Hosono, *Science* **300**, 1269 (2003).
- ³H. Hu, C. X. Zhu, Y. F. Lu, M. F. Li, B. J. Cho, and W. K. Choi, *IEEE Electron Device Lett.* **23**, 514 (2002).
- ⁴J. Robertson, *Rep. Prog. Phys.* **69**, 327 (2006).
- ⁵N. Zhan, K. L. Ng, H. Wong, M. C. Poon, and C. W. Kok, Proceedings of the IEEE Conference Electron Devices and Solid State Circuits, 2003 (unpublished), p. 431.
- ⁶M.-H. Cho, Y. S. Roh, C. N. Whang, K. Jeong, S. W. Nahm, D.-H. Ko, J. H. Lee, N. I. Lee, and K. Fujihara, *Appl. Phys. Lett.* **81**, 472 (2002).
- ⁷H. Harris, K. Choi, N. Mehta, A. Chandolou, N. Biswas, G. Kipshidze, S. Nikishin, S. Gangopadhyay, and H. Temkin, *Appl. Phys. Lett.* **81**, 1065 (2002).
- ⁸R. Thielsch, A. Gatto, J. Heber, and N. Kaiser, *Thin Solid Films* **410**, 86 (2002).
- ⁹J. P. Lehan, Y. Mao, B. G. Bovard, and H. A. Macleod, *Thin Solid Films* **203**, 227 (1991).
- ¹⁰P. Bailey, T. C. Q. Noakes, and D. P. Woodruff, *Surf. Sci.* **426**, 358 (1999).
- ¹¹W.-K. Shih, C.M. Mazier, and A.F. Tasch, *UTQUANT 2.0 User's Guide* (University of Texas, Austin, 1997).
- ¹²C. A. Richter, A. R. Hefner, and E. M. Vogel, *IEEE Electron Device Lett.* **22**, 35 (2001).
- ¹³B. J. O'Sullivan, P. K. Hurley, C. Leveugle, and J. H. Das, *J. Appl. Phys.* **89**, 3811 (2001).
- ¹⁴P. K. Hurley, K. Cherkaoui, E. O'Connor, M. C. Lemme, H. D. B. Gottlob, M. Schmidt, S. Hall, Y. Lu, O. Bui, B. Raeissi, J. Piscator, O. Engstrom, and S. B. Newcomb, *J. Electrochem. Soc.* **155**, G13 (2008).
- ¹⁵M. Schmidt, M. C. Lemme, H. Kurz, T. Witters, T. Schram, K. Cherkaoui, A. Negara, and P. K. Hurley, *Microelectron. Eng.* **80**, 70 (2005).
- ¹⁶G. J. Gerardi, E. H. Poindexter, P. J. Caplan, and N. M. Johnson, *Appl. Phys. Lett.* **49**, 348 (1986).
- ¹⁷A. Stesmans and V. V. Afanas'ev, *Phys. Rev. B* **57**, 10030 (1998).
- ¹⁸A. Stesmans and V. V. Afanas'ev, *Appl. Surf. Sci.* **168**, 324 (2000).
- ¹⁹P. K. Hurley, B. J. O'Sullivan, V. V. Afanas'ev, and A. Stesmans, *Electrochem. Solid-State Lett.* **8**, G44 (2005).

- ²⁰A. H. Al-Bayati, K. G. Orrman-Rossiter, R. Badheka, and D. G. Armour, *Surf. Sci.* **237**, 213 (1990).
- ²¹K. T. Queeney, M. K. Weldon, J. P. Chang, Y. J. Chabal, A. B. Gurevich, J. Sapjeta, and R. L. Opila, *J. Appl. Phys.* **87**, 1322 (2000).
- ²²F. Giustino and A. Pasquarello, *Microelectron. Eng.* **80**, 420 (2005).
- ²³K. Cherkaoui, A. Negara, S. McDonnell, G. Hughes, M. Modreanu, and P. K. Hurley, Proceedings of the 25th International Conference on Microelectronics, 2006, p. 379.
- ²⁴S. Taylor, J. F. Zhang, and W. Eccleston, *Semicond. Sci. Technol.* **8**, 1426 (1993).
- ²⁵H. Kakiuchi, H. Ohmi, M. Harada, H. Watanabe, and K. Yasutake, *Appl. Phys. Lett.* **90**, 151904 (2007).
- ²⁶A. Callegari, E. Cartier, M. Gribelyuk, H. F. Okorn-Schmidt, and T. Zabel, *J. Appl. Phys.* **90**, 6466 (2001).
- ²⁷K. Yamamoto, S. Hayashi, M. Kubota, and M. Niwa, *Appl. Phys. Lett.* **81**, 2053 (2002).
- ²⁸B. Y. Tsui and H. W. Chang, *J. Appl. Phys.* **93**, 10119 (2003).
- ²⁹K. Choi, H. Temkin, H. Harris, S. Gangopadhyay, L. Xie, and M. White, *Appl. Phys. Lett.* **85**, 215 (2004).
- ³⁰D.-Y. Cho, S.-J. Oh, Y. J. Chang, T. W. Noh, R. Jung, and J.-C. Lee, *Appl. Phys. Lett.* **88**, 193502 (2006).
- ³¹C. D. Wagner, W. M. Riggs, L. E. Davis, and J. F. Moulder, *Handbook of X-Ray Photoelectron Spectroscopy*, G. E. Muilenberg, ed. (Perkin-Elmer Corporation (Physical Electronics), 1979) (1st edition).
- ³²R. G. Vitchev, J. J. Pireaux, T. Conard, H. Bender, J. Wolstenholme, and C. Defranoux, *Appl. Surf. Sci.* **235**, 21 (2004).
- ³³M. P. Seah and S. J. Spencer, *Surf. Interface Anal.* **35**, 515 (2003).
- ³⁴F. J. Himpsel, F. R. McFeely, A. Taleb-Ibrahimi, J. A. Yarmoff, and G. Hollinger, *Phys. Rev. B* **38**, 6084 (1988).
- ³⁵S. H. Lo, D. A. Buchanan, Y. Taur, and W. Wang, *IEEE Electron Device Lett.* **18**, 209 (1997).